University of Cape Town

STA5066Z

Mathematical Modelling of Infectious Diseases

Pertussis in the U.S.: A Compartmental Model

Author:
Jared N. Lakhani

Student Number:
LKHJAR001

20 October 2025

Project Repository

Access the source code and project files for this report on GitHub:
https://github.com/LKHJAR001/STA5066Z-Pertussis.git

Contents

1 Introduction

2 Literature Review

2.1 Biology and Transmission Dynamics

Pertussis is a highly contagious respiratory disease caused by the human-adapted, Gram-negative (looks pink/red in the Gram stain) coccobacillus *Bordetella pertussis*. Comparative genomics indicates *B. pertussis* evolved from a *B. bronchiseptica*-like ancestor, adapting to the human nasopharynx (the top part of the throat) (Diavatopoulos et al., 2005). Its pathogenesis (the development of the disease) is driven by adhesins (protein on top of bacteria which allows for attachment) and toxins, notably pertussis toxin (PT) and adenylate cyclase toxin (ACT), which subvert phagocyte (a type of white blood cell which breaks down bacteria) function and promote persistent cough (Carbonetti, 2010).

Transmission occurs primarily via respiratory droplets during close, face-to-face contact. Infectiousness is greatest in the catarrhal phase (basically when it looks like a common cold) and the first two weeks after cough onset; patients are considered non-contagious after five days of appropriate antibiotics Wiuff et al. (2005) (or after 21 days if untreated Wright (1995)). Secondary attack rates among susceptible household contacts are high (often $\sim$80%), underscoring efficient person-to-person spread (Centers for Disease Control and Prevention, 2024a). Inter-epidemic dynamics are cyclical: even in highly vaccinated settings, larger epidemics recur every 3 - 5 years (European Centre for Disease Prevention and Control, 2024).

2.2 History and Current Burden

Before widespread vaccination in the 1940s, pertussis was among the most common childhood diseases in the United States, with >200,000 cases annually and substantial mortality (Centers for Disease Control and Prevention, 2025). Routine immunization drove dramatic declines through the mid-late 20th century. However, multiple countries have observed resurgences since the 1990s, attributed to factors including waning immunity (after both infection and vaccination) and improved detection (Wendelboe et al., 2005).

Globally, a modeling analysis estimated 24.1 million cases and 160,700 deaths among children < 5 years in 2014, with the largest burden in low- and middle-income countries (Yeung et al., 2017). In the post-COVID-19 era, pertussis activity rebounded across Europe; ECDC reported $>$ 25,000 cases in 2023 and $>$ 32,000 cases in just January-March 2024, consistent with the expected 3-5 year periodicity (European Centre for Disease Prevention and Control, 2024). Several countries peaked again in 2024 - 2025, with notable infant morbidity and deaths. U.S. surveillance shows a national peak around Nov 2024 with elevated activity into 2025. Age distributions in recent European outbreaks show high incidence in older children and adolescents, while the most severe outcomes remain concentrated in young infants who are too young to be fully vaccinated.

Spain reported its worst pertussis epidemic in 50 years between $2023 - 2024$ ($28,688$ cases; 920 hospitalizations; 12 deaths), with teens $10 - 14$ years heavily affected - an age shift consistent with waning immunity.

2.3 Control: Treatment, Vaccination, and Immunity

2.3.1 Clinical management and post-exposure prophylaxis

Macrolides (azithromycin, clarithromycin, erythromycin) are the preferred antibiotics for treatment across most ages (Centers for Disease Control and Prevention, 2024d). Early therapy can attenuate symptoms and, critically, curtails infectiousness. For household and other close contacts at elevated risk (infants, pregnant patients), post-exposure prophylaxis (PEP) is recommended, ideally within 21 days of exposure, using the same antibiotic options (Centers for Disease Control and Prevention, 2005). Public health control also includes exclusion from group settings until five full days of effective therapy (or 21 days if untreated) (Centers for Disease Control and Prevention, 2024a).

2.3.2 Vaccination strategies

Routine childhood immunization uses DTaP at $2, 4, 6, 15 - 18$ months, and $4 - 6$ years; adolescents receive a single Tdap dose at $11 - 12$ years; adults who have never received Tdap should receive one dose, with decennial Td/Tdap thereafter for tetanus and diphtheria protection (Centers for Disease Control and Prevention, 2024c). Since infants face the highest risk of hospitalization and death before their primary series, maternal Tdap vaccination during each pregnancy (preferably $27 - 36$ weeks) is a cornerstone policy: CDC evaluations show about 78% effectiveness against pertussis in infants < 2 months and $\sim$ 91% effectiveness against infant hospitalizations (**?**Skoff et al., 2017).

2.3.3 Waning immunity and vaccine performance

Protection following natural infection is not lifelong; model-based inference places the mean duration at $\sim 30-60$ years (Wirsing von Konig, 2005), whereas CDC clinical summaries typically cite $\sim 4 - 20$ years. Vaccine-derived protection also wanes, with estimates of $4 - 12$ years depending on schedule and product (Miller et al., 2014). Observational studies during U.S. outbreaks demonstrated notable waning after the fifth DTaP dose in late childhood (Klein et al., 2012). Modeling work further quantify decline in effectiveness over time, particularly in adolescents (Chit et al., 2018). Maternal, transplacentally (passes through the placenta) acquired anti-pertussis IgG (immunoglobulin G antibodies) wanes rapidly in early infancy, with infant half-lives of approximately $29 - 36$ days after maternal Tdap (Guris et al., 1999).

3 The Dataset

The dataset employed in this study - the weekly Pertussis case counts - was obtained from the CDC's National Notifiable Diseases Surveillance System (NNDSS) Weekly Data portal (Centers for Disease Control and Prevention, 2024b), filtered by disease category. The dataset records the weekly number of reported pertussis cases across all 50 U.S. states from Sunday, January 1, 2022, through Sunday, August 17, 2025, yielding a total of $T = 188$ time periods. For this study, the 50 states are aggregated into the four ($P = 1$) conventional U.S. Census regions: the Northeast ($p = 1$), the Midwest ($p = 2$), the West ($p = 3$), and the South ($p = 4$). Although the dataset does not provide disaggregation by age group, the modeling framework developed in this study explicitly incorporates age structure to address this limitation.

A salient feature of the reported weekly cases across the $P = 4$ regions is the pronounced increase in incidence observed around mid-November 2024 ($t \approx 150$), which we explicitly aim to capture in our model calibration (see Section 6). Moreover, the reported weekly incidence does not exhibit evidence of cyclical patterns, and therefore we do not incorporate seasonality into the force of infection specification in Section 4.1. Nevertheless, as discussed in Section 2, pertussis exhibits multi-annual periodicity with cycles typically spanning $3 - 5$ years. Since our dataset covers fewer than three years, we do not incorporate a seasonality term in the present analysis.

4 The Model

The compartmental pertussis model employed in this study comprises nine compartments and $P = 4$ regions, justified by our dataset which aggregates weekly reported cases at the regional level. To maintain parsimony, the population is stratified into three age groups, $A = 3$: infants (< 1 year), children (1–10 years), and adolescents/adults (> 10 years). This classification reflects distinct epidemiological and immunological profiles: (i) infants face the highest risk of severe pertussis and rely primarily on maternal immunity prior to routine immunization (Centers for Disease Control and Prevention, 2024e); (ii) children (1-10 years) generally remain well protected following the preschool DTaP booster, although waning immunity begins during this period (Klein et al., 2016); and (iii) adolescents and adults experience rapid waning following the Tdap booster and thus serve as reservoirs of transmission (Acosta et al., 2015).

The vaccinated compartment, V, comprises individuals who have received DTaP or Tdap, whereas the maternal-immunity compartment, M, comprises newborns with passively acquired protection from mothers vaccinated with Tdap during pregnancy (Section 2.3.2). Pertussis exhibits a measurable incubation (latent) period - symptoms typically emerge $5 - 10$ days after exposure - and infectiousness peaks during the early catarrhal stage rather than immediately upon infection; accordingly, we include an exposed state E (Bisgard et al., 2004). We also distinguish a population of symptomatic but untreated, $C^{\bar{T}}$, to reflect the frequent mild or atypical presentations in adolescents and adults that delay care and prolong infectiousness (Guris et al., 1999). To capture evidence of subclinical carriage with onward transmission among vaccinated or previously exposed hosts, we also include an asymptomatic infectious class, As (Warfel et al., 2014). The treated class, T, represents symptomatic cases receiving macrolide therapy (Section 2.3.1). Finally, we allow for waning of protection from maternal antibodies, vaccination, and infection-acquired immunity, implemented as transitions $M \to S$, $V \to S$, and $R \to S$ (Section 2.3.3).

Furthermore, each compartment $X \in \{S, M, V, E, As, C^T, C^{\bar{T}}, T, R\}$ exists for each age group a and region p, denoted $X_{a,p}$. An exception is the maternal immunity compartment M, which is defined only for $a = 0$, as elaborated in Section 4.2. For now, all parameters are assumed to be functions of age band $a = 0, \ldots, A - 1$ and region $p = 1, \ldots, P$.

Figure 1 presents the flow diagram of the pertussis model for age group $a = 0$ and any region $p = 1, \ldots, P$ (we note $a = 0$ in Figure 1 since the M population exists as well as births being present). For clarity, flows corresponding to aging, migration, and mortality are excluded (though these are detailed in Sections 4.2, 4.3, and 4.5, respectively), as they apply equivalently to all compartments. We assume that a proportion $\pi_{0,p}$ of newborns have maternal immunity (M), which wanes at rate $\omega^M_{0,p}$, moving individuals into the susceptible population. Susceptible individuals may be vaccinated at rate $v_{a,p}$, entering the vaccinated compartment (V). Vaccinated individuals lose immunity at rate $\omega^V_{a,p}$. Vaccine efficacy is denoted by $\epsilon_{a,p}$, implying that vaccinated individuals may still become exposed at rate $(1 - \epsilon_{a,p})\lambda_{a,p}(t)$, where $\lambda_{a,p}(t)$ denotes the force of infection (see Section 4.1).

The infectious pool consists of the asymptomatic population (As), the symptomatic population whom will not seek treatment ($C^{\bar{T}}$), and the symptomatic population whom will seek treatment (C^T). The parameters $p^A_{a,p}$ and $p^T_{a,p}$ denote the proportions of exposed individuals who become asymptomatic and symptomatic, respectively. Symptomatic population whom will seek treatment (C^T) receive treatment at rate $\tau_{a,p}$, after which entering the treated population (T), which we assume to no longer be infectious, and then recover at rate $\gamma^T_{a,p}$, entering the recovered population ($R_{a,p}$). Asymptomatic individuals recover at rate $\gamma^I_{a,p}$, while symptomatic individuals whom never sought treatment ($C^{\bar{T}}$) first lose symptoms at rate $\delta_{a,p}$ before eventually recovering. Finally, natural immunity wanes at rate $\omega^R_{a,p}$, returning recovered individuals to the susceptible population. Assumptions made for the pertussis model are found in Appendix D.

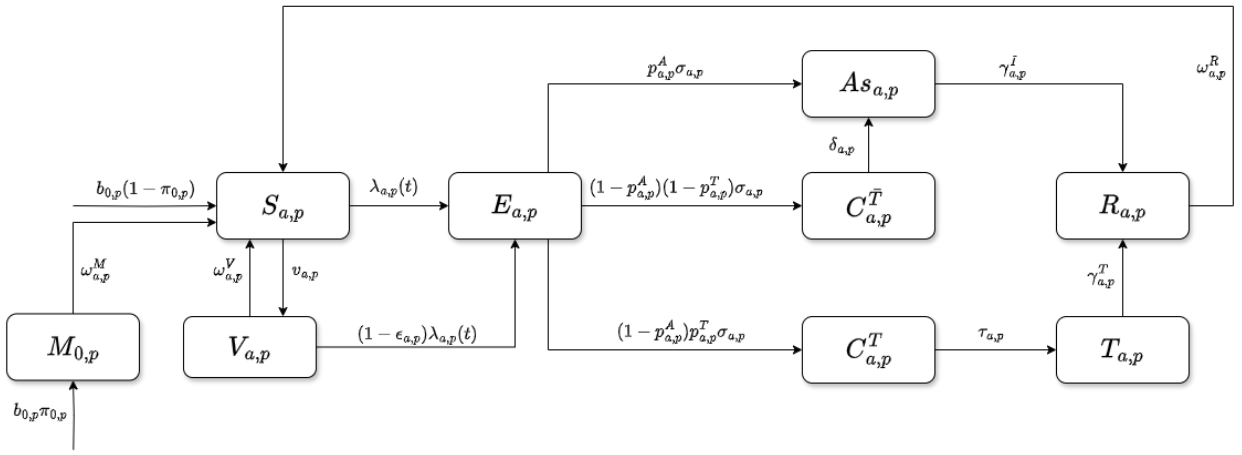

Figure 1: Flow diagram of pertussis model for $a = 0$.

4.1 Force of infection

We define the force of infection - that is, the instantaneous rate at which susceptible individuals in age band a, residing in patch p, at time t acquire infection - as:

$$\lambda_{a,p}(t) \;=\; \beta^0_p\left(1+\beta^1_p \exp\left(-\tfrac{1}{2}\left(\tfrac{t-\phi_p}{\sigma^G_p}\right)^2\right)\right)\frac{\zeta^A_{a,p}As_{a,p} \;+\; \zeta_{a,p}\left(C^{\bar{T}}_{a,p} \;+\; C^T_{a,p}\right)}{N_{a,p}},$$

where β^0_p denotes the baseline transmission rate in region p. The Gaussian bump term, $\left(1+\beta^1_p \exp\left(-\frac{1}{2}\left(\frac{t-\phi_p}{\sigma^G_p}\right)^2\right)\right)$ introduces a localized increase in the force of infection around $t = \phi_p$, with β^1_p representing the amplitude of the perturbation. The parameter σ^G_p governs the spread of the Gaussian bump: larger values correspond to broader, flatter increases. Now since the pertussis dataset provides reported cases only at the regional (rather than age-specific) level, the baseline transmission rates (β^0_p), Gaussian amplitudes (β^1_p), centres (ϕ_p), and widths (σ^G_p) are to only be estimated at the regional level (undergone in Section 6). Finally, we adopt the simplifying assumption that individuals in age band a and patch p mix only within their own group; in other words, cross-age and cross-regional interactions - (a, p) with (a', p') for $a \neq a'$ or $p \neq p'$ - are assumed negligible.

The infectious prevalence term is given by $\frac{\zeta^A_{a,p}A_{a,p}+\zeta_{a,p}\left(C^{\bar{T}}_{a,p}+C^T_{a,p}\right)}{N_{a,p}}$, which denotes the fraction of individuals in group (a, p) who are infectious (we set $\zeta_{a,p} = 1$ to ensure the symptomatic infectious is the reference category). The numerator aggregates all infectious individuals in group (a, p), while the denominator corresponds to the total population size of the group: $N_{a,p} = \mathbb{I}(a = 0) \cdot M_{a,p} + S_{a,p} + V_{a,p} + E_{a,p} + A_{a,p} + C^{\bar{T}}_{a,p} + C^T_{a,p} + T_{a,p} + R_{a,p}$.

Accordingly, the force of infection can be decomposed as:

$$\underbrace{\text{baseline transmission rate}}_{\beta^0} \times \underbrace{\text{Gaussian bump at t} = \phi_p}_{1+\beta^1\exp(\cdot)} \times \underbrace{\text{infectious prevalence in group } (a,p)}_{\text{prevalence term}}.$$

4.2 Aging

We note $\alpha_a = \frac{1}{\text{width of age band } a}$ (hence $\alpha_0 = 1$ years^{-1}, $\alpha_1 = \frac{1}{10}$ years^{-1} and $\alpha_2 = 0$ years^{-1}) , where aging is applied within each patch p and to every compartment $X \in \{S, M, V, E, As, C^T, C^{\bar{T}}, T, R\}$, with rules for M (maternal immunity) and S (susceptible):

- M only exists in the youngest age band ($a = 0$). When infants lose maternal immunity they go to $S_{0,p}$ at rate ω_M.
- If any infants remain in $M_{0,p}$ until they age out of band $a = 0$, they move directly to susceptible in the next age band: $M_{0,p} \xrightarrow{\alpha_0} S_{1,p}$.

4.2.1 Generic aging

For any compartment X, we define:

$$\frac{dX_{a,p}}{dt}\Big|_{\text{aging}} = \begin{cases} -\alpha_a X_{a,p} + \alpha_{a-1}X_{a-1,p}, & 1 \le a \le A-1, \\ -\alpha_0 X_{0,p}, & a = 0, \\ +\alpha_{A-1}X_{A-1,p}, & a = A, \end{cases}$$

which we add to every ODE term.

4.3 Migration

Let patches be $p = 1, \ldots, P$. For each age band a and each compartment $X \in \{S, M, V, E, A, C^T, C^{\bar{T}}, T, R\}$ define migration rates $m_{p\to q}(a) \geq 0 \quad (p \neq q)$, the per-capita rate of moving home from patch p to patch q for age-band a. For every compartment X, we define:

$$\frac{dX_{a,p}}{dt}\Big|_{\text{migration}} = \sum_{q\neq p} m_{q\to p}(a)\, X_{a,q} - \left(\sum_{q\neq p} m_{p\to q}(a)\right) X_{a,p}.$$

which we add to every ODE term. We may view these migration terms in matrices, for $a = 0, \ldots, A-1$:

$$\boldsymbol{Mi}(a) = \begin{bmatrix} 0 & m_{1\to 2}(a) & \cdots & m_{1\to P}(a) \\ m_{2\to 1}(a) & 0 & \cdots & m_{2\to P}(a) \\ \vdots & \vdots & \ddots & \vdots \\ m_{P\to 1}(a) & m_{P\to 2}(a) & \cdots & 0 \end{bmatrix}.$$

4.4 Births

Births may only occur in age band $a = 0$, which adds to the S and M compartment at rate $b_{0,p}(1-\pi_{0,p})$ and $b_{0,p}\pi_{0,p}$ respectively - where $\pi_{0,p}$ denotes the fraction of newborns with maternal immunity, and $b_{0,p}$ denotes the birth rate (for patch p).

4.5 Mortality

We define our mortality rate for age band a for patch p as $\mu_{a,p}$, where for every compartment X there is an outflow of $\mu_{a,p}X_{a,p}$ (which we subtract from every ODE term).

4.6 ODEs

We note the ODE's to be solved for; excluding aging, migration and mortality terms.

$$\begin{aligned}
\frac{dM_{0,p}}{dt} &= \mathbb{I}(a=0)\cdot\left(b_{0,p}\pi_{0,p}N_{0,p} - \omega^M_{0,p}M_{0,p}\right), \\
\frac{dS_{a,p}}{dt} &= \mathbb{I}(a=0)\cdot\left(b_{0,p}(1-\pi_{0,p})N_{0,p} + \omega^M_{0,p}M_{0,p}\right) + \mathbb{I}(a=1)\cdot(\alpha_{0,p}M_{0,p}) + \omega^V_{a,p}V_{a,p} + \omega^R_{a,p}R_{a,p} \\
&\quad - \lambda_{a,p}(t)S_{a,p} - v_{a,p}S_{a,p}, \\
\frac{dV_{a,p}}{dt} &= v_{a,p}S_{a,p} - \omega^V_{a,p}V_{a,p} - (1-\epsilon_{a,p})\lambda_{a,p}(t)V_{a,p}, \\
\frac{dE_{a,p}}{dt} &= \lambda_{a,p}(t)S_{a,p} + (1-\epsilon_{a,p})\lambda_{a,p}(t)V_{a,p} - p^A_{a,p}\sigma_{a,p}E_{a,p} - (1-p^A_{a,p})(1-p^T_{a,p})\sigma_{a,p}E_{a,p} - (1-p^A_{a,p})p^T_{a,p}\sigma_{a,p}E_{a,p}, \\
\frac{dAs_{a,p}}{dt} &= p^A_{a,p}\sigma_{a,p}E_{a,p} + \delta_{a,p}C^{\bar{T}}_{a,p} - \gamma^I_{a,p}As_{a,p}, \\
\frac{dC^{\bar{T}}_{a,p}}{dt} &= (1-p^A_{a,p})(1-p^T_{a,p})\sigma_{a,p}E_{a,p} - \delta_{a,p}C^{\bar{T}}_{a,p}, \\
\frac{dC^T_{a,p}}{dt} &= (1-p^A_{a,p})p^T_{a,p}\sigma_{a,p}E_{a,p} - \tau_{a,p}C^T_{a,p}, \\
\frac{dT_{a,p}}{dt} &= \tau_{a,p}C^T_{a,p} - \gamma^T_{a,p}T_{a,p}, \\
\frac{dR_{a,p}}{dt} &= \gamma^I_{a,p}As_{a,p} + \gamma^T_{a,p}T_{a,p} - \omega^R_{a,p}R_{a,p}.
\end{aligned}$$

Furthermore, we define the incidence of symptomatic pertussis cases as $\frac{dCInc_{a,p}}{dt} = (1-p^A_{a,p})\,p^T_{a,p}\,\sigma_{a,p}\,E_{a,p}$, which represents the flow of individuals in the age band a and patch p who progress from the exposed population to the clinically symptomatic population who seek treatment - we assume that only these individuals contribute to the reported case counts.

5 The Parameters

We specify which parameters introduced in Section 4 are to be estimated directly from the pertussis dataset, and which can be reliably obtained from existing literature. Parameters that retain dependence on age a and region p are represented as $A \times P$ matrices. Similarly, each compartment $X_{a,p}$ may be expressed as an $A\times P$ matrix $\boldsymbol{X}$ encompassing all corresponding compartments.

5.1 Parameters sourced from literature

Rate parameters in Table 1 are typically reported in units of $\frac{1}{\text{day}}$, which we convert to a weekly scale as $\frac{1}{\text{week}} = 7\cdot\frac{1}{\text{day}}$. When rates are reported on an annual basis, we instead apply the conversion $\frac{1}{\text{week}} = \frac{1}{52}\cdot\frac{1}{\text{year}}$. In cases where the literature provides a range of plausible values, we adopt the conservative bound. If absolute rates are displayed, we obtain per-capita rates by dividing the specific absolute rate for group (a,p) by $\text{pop}_{a,p}$. Furthermore, some of the parameter values listed in Table 1 have already been mentioned in Section 2.

Seeing as our dataset starts at the beginning of the year 2022 - it would be more realistic to align these starting values to an already existing state of pertussis in the U.S. Through preliminary experimentation, we observed that the initial values assigned to the vaccinated and recovered populaitons, $\mathbf{V}(0)$ and $\mathbf{R}(0)$ respectively, had a pronounced influence on the scaling of the incidence reported $CInc$. The study was unable to accruatley surmise these populaiton values for the beginning of 2022, so to address this, the study conducts a sensitivity analysis of $\mathbf{V}(0)$ and $\mathbf{R}(0)$ on $CInc$, as presented in Section ??. Furthermore, for this section, we merely assume that the vaccinated and recovered populaiton size is a quarter of the total populaiton: $\boldsymbol{V}(0) = \boldsymbol{R}(0) = \frac{1}{4}\mathbf{pop}$ where $\mathbf{pop}$ denotes the age- and patch-specific population matrix (see Appendix A.1). Furthermore, we set $\boldsymbol{C^T}(0)$ directly from the dataset, corresponding to the number of reported cases in the first week of observation. The maternal, exposed, asymptomatic, untreated symptomatic, and treated compartments are initialised as $\boldsymbol{M}(0) = \boldsymbol{E}(0) = \boldsymbol{A}(0) = \boldsymbol{C^{\bar{T}}}(0) = \boldsymbol{T}(0) = \mathbf{1}_{A\times P}$, representing a minimal seeding of one individual per age band and patch. The susceptible compartment is then determined by population balance: $\boldsymbol{S}(0) = \mathbf{pop} - \Big(\boldsymbol{M}(0) + \boldsymbol{E}(0) + \boldsymbol{A}(0) + \boldsymbol{C^T}(0) + \boldsymbol{C^{\bar{T}}}(0) + \boldsymbol{T}(0) + \boldsymbol{V}(0) + \boldsymbol{R}(0)\Big)$. Furthermore, we assume the sourced parameter values in Table 1 hold for our modelling period of Sunday, January 1, 2022 to Sunday, August 17, 2025 regardless of the year in which they were sourced.

Parameter & Value	**Definition**	**Reference**
$\sigma_{a,p} \approx \frac{1}{5-10}$ days^{-1}	Transition rate from exposed to infectious (Latent Period)$^{-1}$.	Bisgard et al. (2004)
$\gamma^I_{a,p} \approx \frac{1}{21}$ days^{-1}	Clearance rate under no treatment (Infectious period (asymptomatic))$^{-1}$.	Wright (1995)
$\gamma^T_{a,p} \approx \frac{1}{5}$ days^{-1}	Clearance rate under antibiotic treatment (Infectious period (treated))$^{-1}$.	Wiuff et al. (2005)
$p^A_{0,p} \approx 0.1,\ p^A_{1,p} \approx 0.3,\ p^A_{2,p} \approx 0.4-0.6$	Fraction of infections that remain asymptomatic (per age band) - adolescents and adults frequently experience mild or atypical pertussis, whereas infants typically present with classic/severe disease.	Wirsing von Konig (2005)
$p^T_{0,p} \approx 0.8,\ p^T_{1,p} \approx 0.4-0.6,\ p^T_{2,p} \approx 0.4-0.6$	Fraction of symptomatic infections that seek treatment (per age band) - infants experience the most severe disease and the highest hospitalization rates.	Guris et al. (1999)
$\omega^M_{0,p} = \frac{\log(2)}{30}$ days^{-1}	Waning rate of maternal antibodies (half-life $\approx$ 30 days).	Guris et al. (1999)
$\omega^V_{a,p} = \frac{1}{4-12}$ years^{-1}	Rate of loss of vaccine-acquired immunity.	Miller et al. (2014)
$\omega^R_{a,p} = \frac{1}{30-60}$ years^{-1}	Rate of loss of natural immunity.	Wirsing von Konig (2005)
$\zeta^A_{a,p} = 0.3-0.7,\ \ \zeta_{a,p} = 1$	Relative infectiousness of asymptomatic and symptomatic infections - vaccine protection can prevent disease (asymptomatic) while permitting infection. We use symptomatic infectious as reference.	Lavine et al. (2011)
$\tau_{0,p} = \frac{1}{5.6}$ days^{-1},$\tau_{1,p} = \frac{1}{13.8}$ days^{-1},$\tau_{2,p} = \frac{1}{13.8}$ days^{-1}	Reciprocal of mean delay from symptoms onset to appropriate antibiotic treatment	Evans et al. (2023)
$\epsilon_{0,p} = 0.8,\ \epsilon_{1,p} = 0.8,\ \epsilon_{2,p} = 0.5$	Vaccine efficacy: protection conferred by acellular pertussis (aP) vaccines (DTaP for infants/children and Tdap for adolescents/adults) - the reduction in risk of developing symptomatic pertussis disease after vaccination, relative to an unvaccinated individual.	Regan et al. (2018), Klein et al. (2016), Acosta et al. (2015)
$\pi_{0,p} = 0.55$	Fraction of newborns with maternal immunity (coincides with fraction of pregnant women whom've received vaccine).	Centers for Disease Control and Prevention (2024e)
$\delta_{a,p} = \frac{1}{1-6}$ weeks^{-1}	Rate one may exit paroxysmal symptomatic window (the intense-cough period).	Wirsing von Konig (2005)
$\boldsymbol{Mi^*}(a) = \begin{bmatrix} 0 & 410.49 & 410.49 & 410.49 \\ 105.1581 & 0 & 105.16 & 105.16 \\ 362.57 & 362.57 & 0 & 362.57 \\ 0 & 0 & 0 & 0 \end{bmatrix} \frac{\text{average \# persons}}{\text{week}}$	Weekly absolute migration rates where $Mi^*_{p,q}(a)$ denotes the average number of migrants in age band a moving from origin region p to destination region q.	Refer to Appendix A
$\boldsymbol{b}^*_0 = \begin{bmatrix} 11846.24 & 14255.85 & 16390.07 & 27174.64 \end{bmatrix} \frac{\text{average \# persons}}{\text{week}}$	Weekly absolute birth rates for patches $p = 1, \ldots 4$.	Refer to Appendix A

$\boldsymbol{\mu}^* = \begin{bmatrix} 128.34 & 154.45 & 177.57 & 294.41 \\ 1283.44 & 1544.50 & 1775.72 & 2944.14 \\ 9336.79 & 11235.97 & 12918.09 & 21418.11 \end{bmatrix}$ $\frac{\text{average \# persons}}{\text{week}}$	Weekly absolute mortality rates, where $\mu^*_{a,p}$ denotes the average weekly number of deaths in age-band a and region p.	Refer to Appendix A
$\boldsymbol{v}^* = \begin{bmatrix} 1636.90 & 1969.85 & 2264.76 & 3754.95 \\ 16368.96 & 19698.53 & 22647.56 & 37549.52 \\ 119081.31 & 143303.34 & 164757.05 & 273166.23 \end{bmatrix}$ $\frac{\text{\# vaccines}}{\text{week}}$	Weekly absolute vaccination rates where $v^*_{a,p}$ denotes the average weekly number of vaccines given out to age-band a in patch p.	Refer to Appendix A

Table 1: Parameters, definitions, and sources used in the pertussis model.

6 Model Fitting

We estimate the baseline transmission rates (β_p^0), Gaussian amplitudes (β_p^1), Gaussian centres (ϕ_p), Gaussian widths (σ_p^G), and the reporting fractions (ρ_p), where $\rho_p \in [0,1]$ represents the proportion of true infections that are reported. Let $Y_p(t)$ denote the number of reported cases in patch p at week $t = 0, \ldots, T = 187$. Since the pertussis dataset does not specify reported cases by age band, but only at the regional level p, we aggregate over the $A = 3$ age bands: $Y_p(t) = \sum_{a=0}^{A-1} CInc_{a,p}(t)$. We let $\mu_p(t; \boldsymbol{\theta}, \rho_p) = \rho_p Y_p^{\text{Model}}(t; \beta_{1:P}^0, \beta_{1:P}^1, \sigma_{1:P}^G, \phi_{1:P})$ denote the model-predicted mean number of reported cases, where $Y_p^{\text{Model}}(\cdot)$ is the model-predicted incidence before accounting for underreporting. We note that Y_p^{Model} is a function of time as well as all P baseline transmission rates ($\beta_{1:P}^0$), Gaussian amplitudes ($\beta_{1:P}^1$), Gaussian centres ($\phi_{1:P}$), and Gaussian widths ($\sigma_{1:P}^G$). For convenience, we collect these parameters in $\boldsymbol{\theta} = \left[\beta_{1:P}^0, \beta_{1:P}^1, \sigma_{1:P}^G, \phi_{1:P}\right]$.

6.1 Maximum likelihood estimation

6.1.1 Poisson Likelihood

We assume $Y_p(t) \sim \text{Poisson}(\mu_p(t; \boldsymbol{\theta}, \rho_p))$, that is, infection events within a week are treated as independent arrivals at an approximately constant rate $\mu_p(t; \boldsymbol{\theta}, \rho_p) = \rho_p Y_p^{\text{Model}}(t; \boldsymbol{\theta})$, where $Y_p^{\text{Model}}(\cdot)$ denotes the model-predicted incidence prior to accounting for under-reporting. The likelihood for patch p is therefore given by

$$L_p(\boldsymbol{\theta}, \rho_p \mid Y_p(1:T)) = \prod_{t=1}^{T} \frac{\mu_p(t; \boldsymbol{\theta}, \rho_p)^{Y_p(t)} \exp\big(-\mu_p(t; \boldsymbol{\theta}, \rho_p)\big)}{Y_p(t)!}.$$

Taking the logarithm, we obtain the log-likelihood:

$$\begin{aligned} \ell_p(\boldsymbol{\theta}, \rho_p) &= \sum_{t=1}^{T} \left[Y_p(t) \log\big(\mu_p(t; \boldsymbol{\theta}, \rho_p)\big) - \mu_p(t; \boldsymbol{\theta}, \rho_p) - \log\big(Y_p(t)!\big) \right] \\ &\propto \sum_{t=1}^{T} \left[Y_p(t) \log\big(\mu_p(t; \boldsymbol{\theta}, \rho_p)\big) - \mu_p(t; \boldsymbol{\theta}, \rho_p) \right]. \end{aligned}$$

The joint log-likelihood is given by $\ell(\boldsymbol{\Theta}) = \sum_{p=1}^{P} \ell_p(\boldsymbol{\theta}, \rho_p)$ where $\boldsymbol{\Theta} = \left[\boldsymbol{\theta}', \rho_{1:P}\right]'$. Maximum likelihood estimators for the P baseline transmission rates, Gaussian amplitudes, centres, widths, and reporting fractions are obtained by solving $\hat{\boldsymbol{\Theta}}^{\text{MLE}_{\text{Poi}}} = \text{argmax}_{\boldsymbol{\Theta}}\ \ell(\boldsymbol{\Theta})$.

6.1.2 Negative-Binomial likelihood

We assume $Y_p(t) \sim \text{Negative-Binomial}(\mu_p(t; \boldsymbol{\theta}, \rho_p), \kappa_p)$, where $\mu_p(t; \boldsymbol{\theta}, \rho_p)$ denotes the mean, $\kappa_p > 0$ is the dispersion parameter, and $\rho_p \in [0,1]$ is the reporting fraction for patch p. This specification is motivated by the observation that reported case counts typically exhibit greater variability than can be captured by a Poisson distribution. The Negative-Binomial distribution accommodates this overdispersion by introducing the dispersion parameter κ_p, thereby providing a more flexible likelihood. The likelihood for patch p is therefore given by:

$$\begin{aligned} L_p\left(\boldsymbol{\theta}, \rho_p, \kappa_p \mid Y_p(1:T)\right) = \prod_{t=1}^{T} \Bigg[&\frac{\Gamma(Y_p(t) + \kappa_p)}{\Gamma(\kappa_p)\,\Gamma(Y_p(t)+1)} \left(\frac{\kappa_p}{\kappa_p + \mu_p(t; \boldsymbol{\theta}, \rho_p)}\right)^{\kappa_p} \\ &\times \left(\frac{\mu_p(t; \boldsymbol{\theta}, \rho_p)}{\kappa_p + \mu_p(t; \boldsymbol{\theta}, \rho_p)}\right)^{Y_p(t)} \Bigg]. \end{aligned}$$

Taking logarithm, the log-likelihood for patch p becomes:

$$\begin{aligned} \ell_p\left(\boldsymbol{\theta}, \rho_p, \kappa_P\right) = \sum_{t=1}^{T} \Bigg[&\log\left(\Gamma(Y_p(t) + \kappa_p)\right) - \log\left(\Gamma(\kappa_p)\right) - \log\left(\Gamma(Y_p(t)+1)\right) \\ &+ \kappa_p \log\left(\frac{\kappa_p}{\kappa_p + \mu_p(t; \boldsymbol{\theta}, \rho_p)}\right) + Y_p(t)\, \log\left(\frac{\mu_p(t; \boldsymbol{\theta}, \rho_p)}{\kappa_p + \mu_p(t; \boldsymbol{\theta}, \rho_p)}\right) \Bigg]. \end{aligned}$$

The joint log-likelihood is then defined as $\ell(\boldsymbol{\Theta}) = \sum_{p=1}^{P} \ell_p(\boldsymbol{\theta}, \rho_p, \kappa_p)$, where $\boldsymbol{\Theta} = \left[\boldsymbol{\theta}', \rho_{1:P}, \kappa_{1:P}\right]'$. Maximum likelihood estimators for the P baseline transmission rates, Gaussian amplitudes, centres and widths, P reporting fractions, and P dispersion parameters are obtained by solving $\hat{\boldsymbol{\Theta}}^{\text{MLE}_{\text{NB}}} = \text{argmax}_{\boldsymbol{\Theta}}\, \ell(\boldsymbol{\Theta})$.

6.2 Least-squares estimation

Using the same notation as previously, and aiming to minimise the squared differences between the model-predicted means $\mu_p(t; \boldsymbol{\theta}, \rho_p)$ and the observed values $Y_p(t)$ for all $p = 1, \ldots, P$ and $t = 0, \ldots, T$, we define the patch-specific sum of squared errors as $SSE_p(\boldsymbol{\theta}, \rho_p) = \sum_{t=1}^{T} \left(Y_p(t) - \mu_p(t; \boldsymbol{\theta}, \rho_p)\right)^2$. The overall criterion function is then given by $SSE(\boldsymbol{\Theta}) = \sum_{p=1}^{P} SSE_p(\boldsymbol{\theta}, \rho_p)$. where $\boldsymbol{\Theta} = \left[\boldsymbol{\theta}', \rho_{1:P}\right]'$. We obtain the least-squares estimators for the P baseline transmission rates, Gaussian amplitudes, centres, widths, and reporting fractions by solving $\hat{\boldsymbol{\Theta}}^{\text{SSE}} = \text{argmin}_{\boldsymbol{\Theta}}\ SSE(\boldsymbol{\Theta})$.

Figure 2 displays the predicted mean number of reported weekly infections $\hat{\mu}_p(t) = \mu_p\left(t; \hat{\boldsymbol{\theta}}, \hat{\rho}_p\right) = \hat{\rho}_p\, \hat{Y}_p\left(t; \hat{\beta}^0_{1:P}, \hat{\beta}^1_{1:P}, \hat{\sigma}^G_{1:P}, \hat{\phi}_{1:P}\right)$, compared against the observed weekly counts $Y_p(t)$ for each of the four U.S. regions: Northeast ($p = 1$), Midwest ($p = 2$), West ($p = 3$), and South ($p = 4$). The estimates were obtained using the three approaches: (i) maximum likelihood under a Poisson likelihood ($\hat{\boldsymbol{\Theta}}^{\text{MLE}_{\text{Poi}}}$), (ii) maximum likelihood under a Negative Binomial likelihood ($\hat{\boldsymbol{\Theta}}^{\text{MLE}_{\text{NB}}}$), and (iii) least-squares estimation ($\hat{\boldsymbol{\Theta}}^{\text{SSE}}$). Parameter estimates for the P baseline transmission rates, Gaussian amplitudes, widths, centres, and reporting fractions are reported in Tables 2 and 3 in Appendix B.

We find that the estimates obtained under $\hat{\boldsymbol{\Theta}}^{\text{SSE}}$ and $\hat{\boldsymbol{\Theta}}^{\text{MLE}_{\text{Poi}}}$ are numerically identical, which is most likely attributable to the use of identical initial values in the optimisation procedures for both approaches. The study further notes that the resulting estimates were strongly dependent on the initial values used in the optimisation routine. Importantly, only $\hat{\boldsymbol{\Theta}}^{\text{SSE}}$ and $\hat{\boldsymbol{\Theta}}^{\text{MLE}_{\text{Poi}}}$ yielded fitted trajectories $\hat{\mu}_p(t)$ that successfully captured the sharp rise in incidence around $t \approx 150$ weeks (with subsequent decline). By contrast, the estimates under the Negative Binomial likelihood, $\hat{\boldsymbol{\Theta}}^{\text{MLE}_{\text{NB}}}$, produced fitted mean trajectories that failed to capture the post-peak decline in reported cases. Instead, the fitted paths increased monotonically, effectively modelling the observed data $Y_p(t)$ as a continuing growth process rather than one with a distinct peak and decline at $t \approx 150$. Although the 95% prediction intervals under $\hat{\boldsymbol{\Theta}}^{\text{MLE}_{\text{NB}}}$ covered most of the observed data $Y_p(t)$, the predictive mean did not replicate the observed data's structure.

Additionally, across all three estimation approaches, the reporting fractions were consistently estimated at $\hat{\rho}_p \approx 1$ for all $p = 1, \ldots, P$ regions. This outcome likely reflects that the model already possesses adequate parameterization (for example, the Gaussian bump term in the force of infection) to capture the peaks of $Y_p(t)$, thereby rendering the reporting fraction ρ_p largely superfluous.

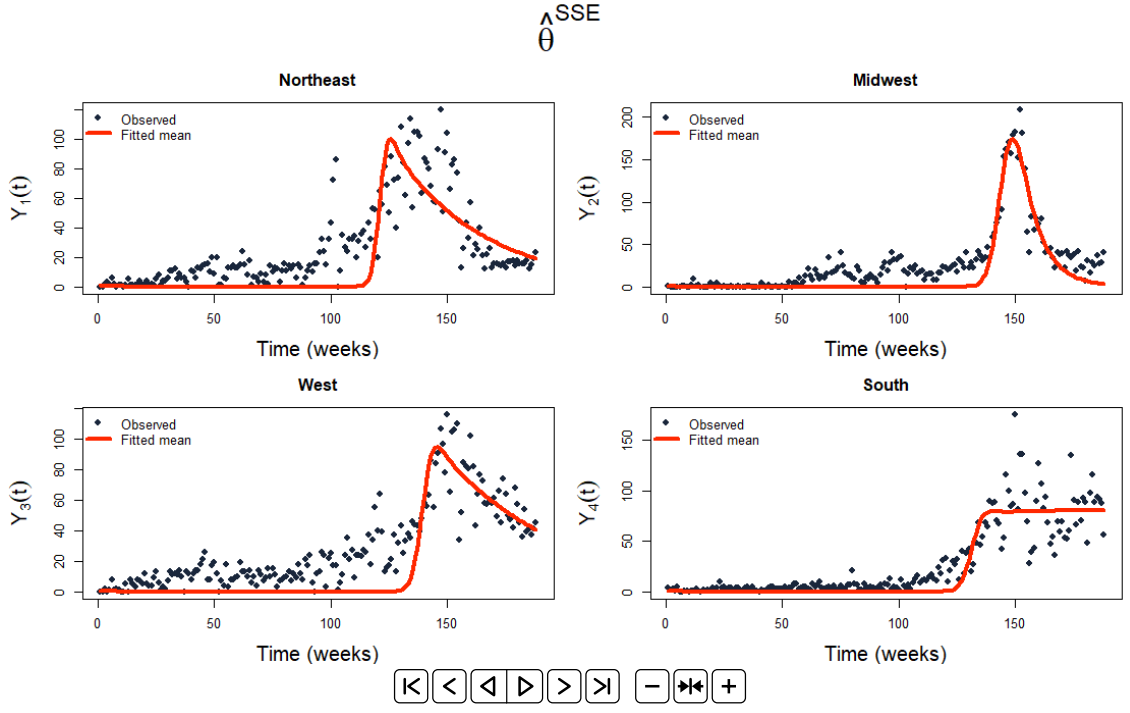

Figure 2: Number of reported weekly infections $Y_p(t)$ and predicted mean number of reported weekly infections $\hat{\mu}_p$ (including prediction intervals) using $\hat{\boldsymbol{\Theta}}^{\text{SSE}}$, $\hat{\boldsymbol{\Theta}}^{\text{MLE}_{\text{Poi}}}$ and $\hat{\boldsymbol{\Theta}}^{\text{MLE}_{\text{NB}}}$ for the $P = 4$ regions.

7 Sensitivity Analysis

We conduct a sensitivity analysis with respect to the initial conditions $\boldsymbol{V}(0)$ and $\boldsymbol{R}(0)$, the P baseline transmission rates β^0_p, and the P Gaussian centres ϕ_p (done in Appendix C), focusing on their influence on the peaks of the predicted mean number of reported

weekly infections $\hat{\mu}_p(t) = \mu_p\big(t; \hat{\boldsymbol{\theta}}, \hat{\rho}_p\big) = \hat{\rho}_p \hat{Y}_p\Big(t; \hat{\beta}^0_{1:P}, \hat{\beta}^1_{1:P}, \hat{\sigma}^G_{1:P}, \hat{\phi}_{1:P}\Big)$. Given that Section 6 specifically aimed to capture the pronounced increase in incidence observed around mid-November 2024, it is natural to summarise the outcomes of the sensitivity analysis in terms of the peaks of the predicted mean number of reported weekly infections $\max\{\hat{\mu}_p\}$ for $p = 1, \ldots, P$.

For this analysis, we employ all parameter values specified in Section 5, together with the estimates $\hat{\boldsymbol{\Theta}}^{\text{SSE}}$ obtained in Section 6.2, in order to generate the P baseline transmission rates, Gaussian amplitudes, centres, widths, and reporting fractions. Furthermore, we note that $\hat{\mu}_p$ denotes the predicted mean number of weekly infections obtained under perturbed parameter values, whereas $\hat{\mu}^*_p$ denotes the baseline predicted mean number of weekly infections - namely, the predicted peak values as calculated in Section 6 using $\hat{\boldsymbol{\Theta}}^{\text{SSE}}$: $\hat{\mu}^*_p = [100.1, 174.7, 94.7, 80.3]$.

7.1 Initial values

We conduct a sensitivity analysis of the initial vaccinated and recovered populations, denoted $\mathbf{V}(0)$ and $\mathbf{R}(0)$, respectively, on the peak of the predicted mean number of weekly reported infections, $\max\{\hat{\mu}_p\}$.

Figure 3 displays heatmaps, for the $p = 1, \ldots, P$ U.S. regions, of $\log\left(\max\left\{\frac{\hat{\mu}_p}{\hat{\mu}^*_p}\right\}\right)$, evaluated across varying values of ρ^V and ρ^R such that $\mathbf{V}(0) = \rho^V \, \mathbf{pop}$ and $\mathbf{R}(0) = \rho^R \, \mathbf{pop}$, subject to the constraint $\rho^V + \rho^R = 0.9$. Negative values on the heatmap indicate that $\max\{\hat{\mu}_p\} < \max\{\hat{\mu}^*_p\}$. We retain the constraint from Section 5 that the susceptible population is given by the population balance $\mathbf{S}(0) = \mathbf{pop} - \Big(\mathbf{M}(0) + \mathbf{E}(0) + \mathbf{A}(0) + \mathbf{C}^T(0) + \mathbf{C}^{\bar{T}}(0) + \mathbf{T}(0) + \mathbf{V}(0) + \mathbf{R}(0)\Big)$, with all other initial populations identical to those specified in Section 5.

Across all regions, the heatmaps reveal that $\log\left(\max\left\{\frac{\hat{\mu}_p}{\hat{\mu}^*_p}\right\}\right)$ decreases as ρ^V and ρ^R increase. This indicates that a smaller initial susceptible population $\mathbf{S}(0)$ produces a smaller peak in the predicted mean number of weekly reported infections. This result is intuitive: a reduced susceptible pool leads to fewer exposures, thereby limiting the number of infections.

Moreover, Figure 3 suggests that $\max\{\hat{\mu}_p\}$ is minimized when $\rho^R \approx 0.9$. That is, when a large fraction of the population begins in the recovered compartment, the predicted peak in reported infections is lowest. This is consistent with the model structure, since the recovered population contributes to the susceptible pool only through waning natural immunity, which we approximated as $\omega^R_{a,p} \approx \frac{1}{30-60}$ years^{-1}. By contrast, when $\rho^V \approx 0.9$, the peak $\hat{\mu}_p$ is also reduced (relative to the baseline $\hat{\mu}^*_p$), though not as dramatically as in the case of large ρ^R. This follows because the vaccinated population contributes to the susceptible pool not only through waning immunity, $\omega^V_{a,p} \approx \frac{1}{4-12}$ years^{-1}, but also directly to the exposed population by infection through vaccine inefficacy. In summary, a large initial recovered population yields a lower predicted peak in infections than an equivalently large initial vaccinated population.

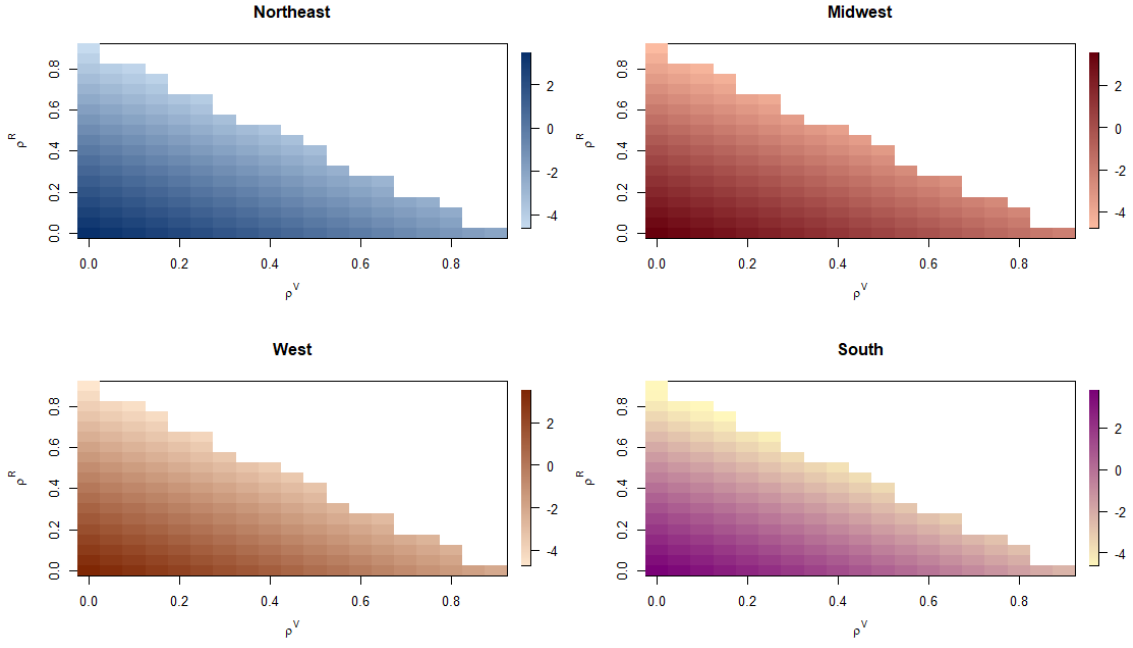

Figure 3: Heatmaps of $\log\left(\max\left\{\frac{\hat{\mu}_p}{\hat{\mu}^*_p}\right\}\right)$ for varying ρ^R and ρ^V for $p = 1, \ldots, P$ regions.

7.2 Baseline transmission rates β^0_p

We additionally conduct a sensitivity analysis of the baseline transmission rates $\hat{\beta}^0_p$ on the peaks of the predicted mean number of reported weekly infections across the $p = 1, \ldots, 4$ regions. For each region p, we summarize the effect using $\log\left(\max\left\{\frac{\hat{\mu}_p}{\hat{\mu}^*_p}\right\}\right)$. Specifically, we vary $\hat{\beta}^0_p$ multiplicatively by a scaling factor $\rho^{\hat{\beta}^0_p} \in [0.5, 1.5]$; that is, we consider fractions and multiples of the baseline transmission estimates reported in Section **??**.

Figure 4 illustrates the influence of varying $\hat{\beta}_p^0$ on the peaks of the predicted mean number of reported weekly infections. We note that migration and its relative values play a large role in how $\rho^{\hat{\beta}_p^0}$ influences said peaks: since there is no outlfow of migrants from the South, the bottom right plot of Figure 4 illustrates that changing $\hat{\beta}_4^0$ has no impact on the peaks in the Northeast $\max\{\hat{\mu}_1\}$, the Midwest $\max\{\hat{\mu}_2\}$ nor the West $\max\{\hat{\mu}_3\}$, but only on the South's peak $\max\{\hat{\mu}_4\}$. That is to say, increasing $\hat{\beta}_4^0$ naturally increases the baseline force of infection for the South region, thereby increasing the peak of the predicted mean number of reported weekly infections.

By contrast, the Northeast (top-left plot in Figure 4) exhibits the largest outflow; increasing $\hat{\beta}_1^0$ raises peak values in all other regions (including its own peak). The West (bottom-left plot) has the second-largest outflow, and increases in $\hat{\beta}_3^0$ likewise elevate peaks elsewhere. Furthermore, the Midwest (top-right plot) has near-negligible migration outflow - hence why increasing $\hat{\beta}_2^0$ has negligible influence in increasing the peaks of the other three regions.

Furthermore, we note that changes in $\hat{\beta}_p^0$ had a negligible effect on the timing of the peaks for the $p = 1, \ldots, P$: $\max_t\{\hat{\mu}_1(t)\}$, $\max_t\{\hat{\mu}_2(t)\}$, $\max_t\{\hat{\mu}_3(t)\}$ and $\max_t\{\hat{\mu}_4(t)\}$.

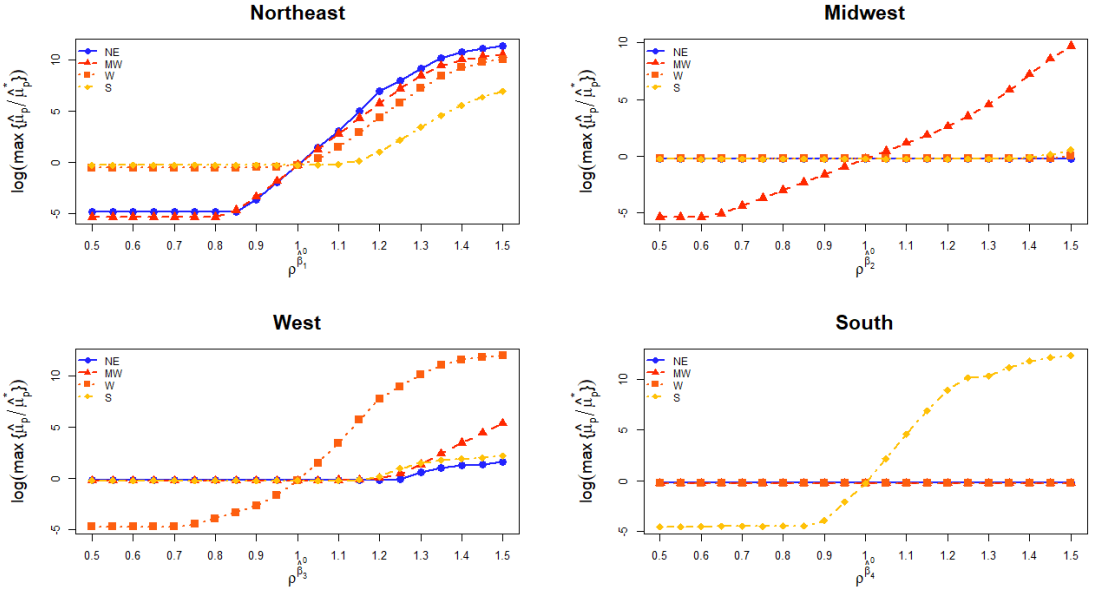

Figure 4: $\log\left(\max\left\{\frac{\hat{\mu}_p}{\hat{\mu}_p^*}\right\}\right)$ vs $\rho^{\hat{\beta}_p^0}$ for $p = 1, \ldots, P$ regions.

8 Introducing Drug Resistance

Because pertussis treatment relies on macrolides for both treatment and PEP, we extend the infectious-treatment pathway with a resistant class $C_{a,p}^{T,\text{Res}}$. Macrolide-resistant *Bordetella pertussis* has been documented, typically via an A2047G mutation in the 23S rRNA gene; resistance is widespread in parts of mainland China and sporadic but reported elsewhere (Feng et al., 2021) - regardless, even though we have U.S data, we entertain the possibility that a macrolide resistant population may exist in the U.S.

This section further investigates how this added $C_{a,p}^{T,\text{Res}}$ population may affect the peaks of the predicted mean number of reported weekly infections $\max\{\hat{\mu}_p\}$. We display the updated pertussis model in Figure 5.

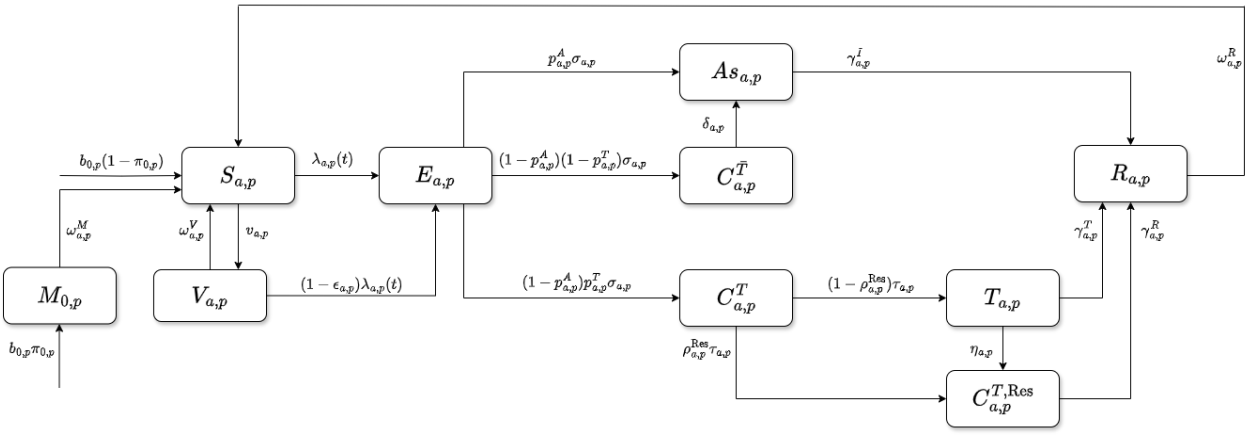

Figure 5: Flow diagram of pertussis model with drug resistance for $a = 0$.

To capture both primary and acquired drug resistance, we extend the treatment pathway with an additional resistant compartment $C_{a,p}^{T,\text{Res}}$. We introduce two new parameters:

- ρ^{Res}: the proportion of clinical cases entering treatment who are already resistant (primary resistance). When individuals in $C^T_{a,p}$ progress, a fraction $(1-\rho^{\text{Res}})$ transition to the standard treated class $T_{a,p}$, while a fraction ρ^{Res} transition directly into $C^{T,\text{Res}}_{a,p}$.
- $\eta_{a,p}$: the rate of acquiring resistance during treatment (acquired resistance). This term moves individuals from $T_{a,p}$ into $C^{T,\text{Res}}_{a,p}$. Resistant infections remain infectious under macrolide therapy - $C^{T,\text{Res}}$ does not enter the noninfectious treated population T). Nor do we assume $C^{T,\text{Res}}$ may switch to an effective alternative treatment (TMP-SMX for example) and move back to $T_{a,p}$

Recovery rates are distinguished by treatment type: $\gamma^T_{a,p}$ for individuals under effective treatment, and $\gamma^R_{a,p}$ for resistant treatment cases, where typically $\gamma^R_{a,p} < \gamma^T_{a,p}$ to reflect poorer outcomes. The modified system is:

$$\begin{aligned}
\frac{dC^T_{a,p}}{dt} &= (1-p^A_{a,p})p^T_{a,p}\sigma_{a,p}E_{a,p} - (1-\rho^{\text{Res}}_{a,p})\tau_{a,p}C^T_{a,p} - \rho^{\text{Res}}_{a,p}\tau_{a,p}C^T_{a,p},\\
\frac{dT_{a,p}}{dt} &= (1-\rho^{\text{Res}}_{a,p})\tau_{a,p}C^T_{a,p} - \gamma^T_{a,p}T_{a,p} - \eta_{a,p}T_{a,p},\\
\frac{dC^{T,\text{Res}}_{a,p}}{dt} &= \rho^{\text{Res}}_{a,p}\tau_{a,p}C^T_{a,p} + \eta_{a,p}T_{a,p} - \gamma^R_{a,p}C^{T,\text{Res}}_{a,p}\\
\frac{dR_{a,p}}{dt} &= \gamma^I_{a,p}As_{a,p} + \gamma^T_{a,p}T_{a,p} + \gamma^R_{a,p}C^{T,\text{Res}}_{a,p} - \omega^R_{a,p}R_{a,p}.
\end{aligned}$$

in addition to the ODEs (where some have been replaced) in Section 4.6. Additionally, we assume the population who are drug resistant $C^{T,\text{Res}}_{a,p}$ remains infectious, hence the prevalence term in Section 4.1 for the force of infection becomes $\frac{\zeta^A_{a,p}A_{a,p}+\zeta_{a,p}\left(C^{\bar{T}}_{a,p}+C^T_{a,p}+C^{T,\text{Res}}_{a,p}\right)}{N_{a,p}}$.

As previously mentioned, primary resistance of *Bordetella pertussis* to macrolides remains a rarity outside of East Asia (Feng et al., 2021). Accordingly, we fix the prevalence of primary resistance at $\rho^{\text{Res}} \approx 0.1\%$ to reflect low background levels in the U.S. Evidence for acquired resistance during therapy is even weaker, with no systematic reports of acquired resistance emerging under macrolide treatment Wang et al. (2021). We therefore set $\eta_{a,p}$ near zero - $\eta_{a,p} = \frac{1}{50}$ days^{-1}. Given the lack of strong evidence for acquired resistance, we simply assign a resistant recovery rate of $\gamma^R_{a,p} = \frac{1}{10}$ days^{-1}, which ensures $\gamma^R_{a,p} < \gamma^T_{a,p}$.

We employ all parameters introduced in Section 5, together with $\hat{\boldsymbol{\Theta}}^{\text{SSE}}$ from Section 6.2, to obtain estimates of the P baseline transmission rates, Gaussian amplitudes, centres, widths, and reporting fractions. This allows us to examine the effect of drug resistance on the peaks of the predicted mean number of weekly reported cases, $\hat{\mu}_p = \mu_p(t;\hat{\boldsymbol{\theta}},\hat{\rho}_p) = \hat{\rho}_p\hat{Y}_p\left(t;\hat{\beta}^0_{1:P},\hat{\beta}^1_{1:P},\hat{\sigma}^G_{1:P},\hat{\phi}_{1:P}\right)$ for each p^{th} region. Figure 6 demonstrates that incorporating drug resistance increases $\hat{\mu}_p$ across the entire time horizon $t \in [0, 187]$, most visibly in intervals where $\hat{\mu}_p(t) \neq 0$. This arises from the force-of-infection term, which now includes an additional infectious compartment: the clinically symptomatic drug-resistant individuals, $C^{T,\text{Res}}_{a,p}$. Moreover, the treated population $T_{a,p}$ is now partitioned into a drug-resistant subpopulation that remains infectious (whereas in Section 4.1 we assumed the treated population to be non-infectious and excluded it from the prevalence term). This expansion of the infectious pool explains the overall increase in the force of infection $\lambda_{a,p}(t)$, which manifests as an upward shift in $\hat{\mu}_p(t)$ in Figure 6.

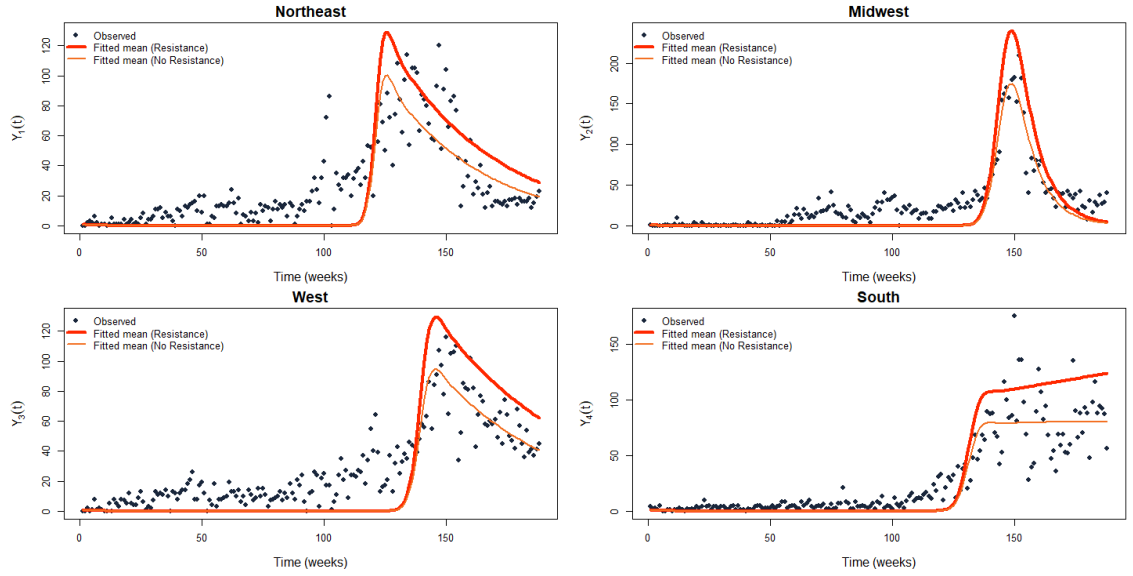

Figure 6: Number of reported weekly infections $Y_p(t)$ and predicted mean number of reported weekly infections $\hat{\mu}_p$ using $\hat{\boldsymbol{\Theta}}^{\text{SSE}}$ for pertussis model with and without drug resistance for the $P = 4$ regions.

Figure 7 illustrates how variation in the proportion of clinical cases entering treatment who are already resistant, ρ^{Res}, as well as the rate of acquiring resistance during treatment, $\eta_{a,p}$, affects the peaks of the predicted mean number of weekly reported cases. We retain the notation that $\hat{\mu}_p$ denotes the predicted mean number of weekly infections under perturbed parameter values, while $\hat{\mu}^*_p$ denotes the baseline predicted mean number of weekly infections - namely, the peak values obtained in Section 6 using $\hat{\boldsymbol{\Theta}}^{\text{SSE}}$.

It is evident from Figure 7 that the peak values of $\hat{\mu}_p$ are strongly influenced by both the size of the $C_{a,p}^{T,\text{Res}}$ population and the rate at which individuals enter this compartment. When the average time required to develop resistance during treatment, given by $\frac{7}{\eta_{a,p}}$, increases, individuals transition more slowly into $C_{a,p}^{T,\text{Res}}$, thereby reducing the infectious population. Similarly, a lower fraction ρ^{Res} of individuals who are already resistant upon entering treatment reduces $C_{a,p}^{T,\text{Res}}$, again lowering the infectious population and consequently decreasing the peak value of $\hat{\mu}_p$. Both an increased $\frac{7}{\eta_{a,p}}$ and a reduced ρ^{Res} correspond to values of $\log\left(\max\left\{\frac{\hat{\mu}_p}{\hat{\mu}_p^*}\right\}\right) \approx 0$ (as seen in the top-left region of the plots in Figure 7 where the average time to develop resistance is ≈ 200 days), indicating that the peaks obtained under perturbed parameters are approximately equal to those obtained under the baseline parameters.

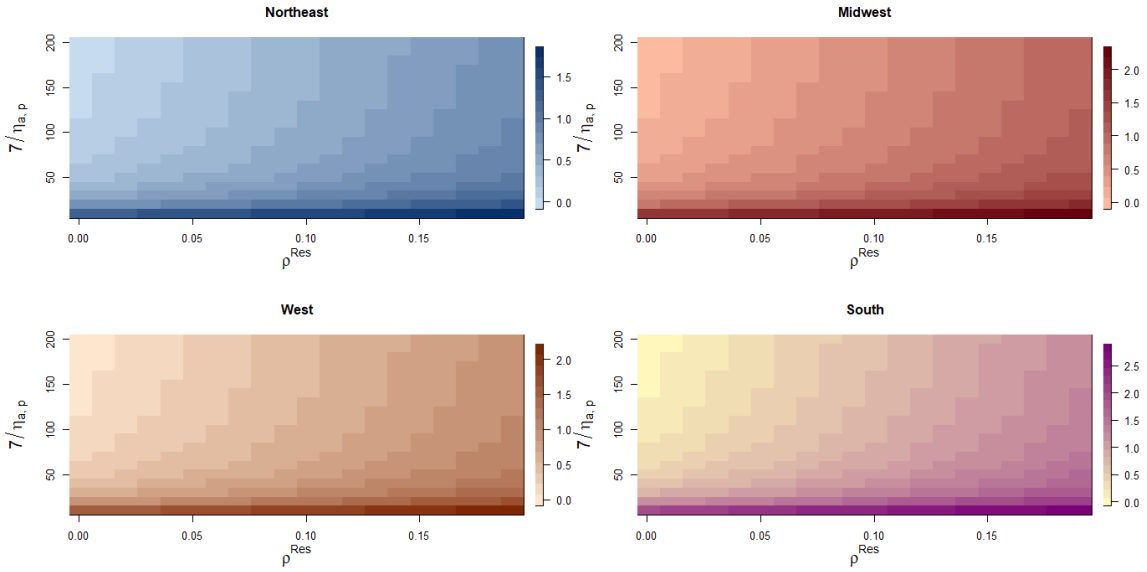

Figure 7: $\log\left(\max\left\{\frac{\hat{\mu}_p}{\hat{\mu}_p^*}\right\}\right)$ vs $\frac{7}{\eta_{a,p}}$ (representing the average number of days it takes to develop drug resistance) and ρ^{Res} for $p = 1, \ldots, P$ regions.

9 Conclusion

Appendices

A Parameter Approximations

A.1 Population Matrix

The corresponding regional population estimates (mid-2024) are as follows:

$$\text{pop}_{p=1} = 57{,}832{,}935, \quad \text{pop}_{p=2} = 69{,}596{,}584, \quad \text{pop}_{p=3} = 80{,}015{,}776, \quad \text{pop}_{p=4} = 132{,}665{,}693,$$

in accordance to U.S. Census Bureau (2024a). Furthermore, the U.S. population under age 18 was estimated at 73.1 million as of July 1, 2024 in accordance with U.S. Census Bureau (2024a). For simplicity, we assume the population under 18 is uniformly distributed across ages. This implies that approximately 4.06 million are infants (< 1), 40.6 million are aged 1-10, and the remaining 295.5 million are aged 10+. We calculate the population sizes per age band $a = 0, 1, 2$ and patch $p = 1, 2, 3, 4$ denoted as $\text{pop}_{a,p}$ as follows:

$$\text{pop}_{0,p} = \sum_{p'} \text{pop}_{p'} \times \frac{\text{pop}_p}{\sum_{p'} \text{pop}_{p'}} \times \frac{1}{18} \frac{\text{pop}_{<18}}{\sum_{p'} \text{pop}_{p'}},$$

$$\text{pop}_{1,p} = \sum_{p'} \text{pop}_{p'} \times \frac{\text{pop}_p}{\sum_{p'} \text{pop}_{p'}} \times \frac{10}{18} \frac{\text{pop}_{<18}}{\sum_{p'} \text{pop}_{p'}},$$

$$\text{pop}_{2,p} = \sum_{p'} \text{pop}_{p'} \times \frac{\text{pop}_p}{\sum_{p'} \text{pop}_{p'}} \times \frac{\left(\sum_{p'} \text{pop}_{p'} - \text{pop}_{<11}\right)}{\sum_{p'} \text{pop}_{p'}},$$

for $p = 1, 2, 3, 4$, where pop_p is the mid-2024 population of region p, and $\text{pop}_{<18} = 73{,}100{,}000$. We define $\text{pop}_{<11} \equiv \frac{11}{18}\text{pop}_{<18}$ as the population aged 0–10. Now $\mathbf{pop} = \begin{bmatrix} \text{pop}_{1,1} & \text{pop}_{1,2} & \text{pop}_{1,3} & \text{pop}_{1,4} \\ \text{pop}_{2,1} & \text{pop}_{2,2} & \text{pop}_{2,3} & \text{pop}_{2,4} \\ \text{pop}_{3,1} & \text{pop}_{3,2} & \text{pop}_{3,3} & \text{pop}_{3,4} \end{bmatrix}$.

A.2 Births

The total number of births in 2024 is reported as $B_{\text{US}} = 3{,}622{,}673$ as per Centers for Disease Control and Prevention (CDC) (2025a) - which we assume to be the yearly absolute birth rate. We approximate the weekly absolute birth rate per region by distributing the yearly absolute birth rate in proportion to the mid-2024 Census population estimates for each region, and dividing by 52, as such:

$$b^*_{0,p} = \frac{B_{\text{US}}}{52} \times \frac{\text{pop}_p}{\sum_{p'} \text{pop}_{p'}}.$$

We then obtain the weekly per-capita birth rate per region as such: $b_{0,p} = \frac{b^*_{0,p}}{\text{pop}_{0,p}}$ for $p = 1, \ldots, P$.

A.3 Mortality

The total number of deaths in 2024 is provisionally reported as $D_{\text{US}} = 3{,}287{,}000$ in accordance with Centers for Disease Control and Prevention (CDC) (2025b) - which we assume to be the yearly absolute mortality rate. We approximate the weekly absolute mortality rate per age by distributing the yearly absolute mortality rate in proportion to the mid-2024 Census population estimates for each age, and dividing by 52. Furthermore, we approximate the weekly absolute mortality rates per age and region, by distributing the weekly absolute mortality rates per age in proportion to the mid-2024 Census population estimates for each region as such:

$$\begin{aligned}
\mu^*_{0,p} &= \frac{D_{\text{US}}}{52} \times \frac{\text{pop}_p}{\sum_{p'} \text{pop}_{p'}} \times \frac{1}{18} \frac{\text{pop}_{<18}}{\sum_{p'} \text{pop}_{p'}}, \\
\mu^*_{1,p} &= \frac{D_{\text{US}}}{52} \times \frac{\text{pop}_p}{\sum_{p'} \text{pop}_{p'}} \times \frac{10}{18} \frac{\text{pop}_{<18}}{\sum_{p'} \text{pop}_{p'}}, \\
\mu^*_{2,p} &= \frac{D_{\text{US}}}{52} \times \frac{\text{pop}_p}{\sum_{p'} \text{pop}_{p'}} \times \frac{\left(\sum_{p'} \text{pop}_{p'} - \text{pop}_{<11}\right)}{\sum_{p'} \text{pop}_{p'}},
\end{aligned}$$

for $p \in \{1, 2, 3, 4\}$. We then obtain the weekly per-capita mortality rate per age and region as such $\mu_{a,p} = \frac{\mu^*_{a,p}}{\text{pop}_{a,p}}$ for $p = 1, \ldots, P$ and $a = 0, 1, 2$.

A.4 Migration

To represent migration flows between Census regions, we utilize U.S. Census Bureau Vintage 2024 estimates of net domestic migration for the period July 2023–June 2024 as per U.S. Census Bureau (2024b). The reported regional net flows are: Northeast $-192{,}109$, Midwest $-49{,}214$, West $-169{,}681$ and South $+411{,}004$ - which we take as yearly absolute migration rates. Since these statistics provide only net changes, the bilateral migration flows must be approximated. We therefore impose a uniform redistribution assumption, whereby each region experiencing net out-migration allocates its outflow equally among the remaining three regions. For instance, the Northeast's net outflow of 192,109 for the year is distributed as $\frac{1}{3} \times 192{,}109 = 64{,}036$ migrants to each of the Midwest, West and South. Additionally, we assume these migration rates are uniform across the age-bands, hence the weekly absolute migration rates per age is given as:

$$\begin{aligned}
m^*_{1\to p'}(a) &= \frac{192109}{52} \times \frac{1}{3} \times \frac{1}{3}, && \text{for } p' \in \{2, 3, 4\}, \\
m^*_{2\to p'}(a) &= \frac{49214}{52} \times \frac{1}{3} \times \frac{1}{3}, && \text{for } p' \in \{1, 3, 4\}, \\
m^*_{3\to p'}(a) &= \frac{169681}{52} \times \frac{1}{3} \times \frac{1}{3}, && \text{for } p' \in \{1, 2, 4\}.
\end{aligned}$$

for $a = 0, 1, 2$. We then obtain the weekly per-capita migration rates as such, $m_{p\to p'}(a) \frac{m^*_{p\to p'}(a)}{\text{pop}_p}$ for $p = 1, \ldots, P$.

A.5 Vaccination

Over the period 2006-2017, a total of 503,068,145 doses of pertussis-containing vaccines (including DT, DTaP, and Tdap) were administered in the United States as per U.S. Health Resources and Services Administration (2018). For modeling purposes, we assume doses are distributed uniformly over this 12-year horizon, yielding an average of $V_{\text{tot}} = \frac{1}{12} \times 503{,}068{,}145 \approx 41.9$ million doses per year - which we assume to be the yearly absolute vaccination rate. We approximate the weekly absolute vaccination rate per age by distributing the yearly absolute vaccination rate in proportion to the mid-2024 Census population estimates for each age, and dividing by 52. Furthermore, we approximate the weekly absolute vaccination rates per age and region, by distributing the weekly absolute vaccination rates per age in proportion to the mid-2024 Census population estimates for each region as such:

$$\begin{aligned}
v^*_{0,p} &= \frac{V_{\text{tot}}}{52} \times \frac{\text{pop}_p}{\sum_{p'} \text{pop}_{p'}} \times \frac{1}{18} \frac{\text{pop}_{<18}}{\sum_{p'} \text{pop}_{p'}}, \\
v^*_{1,p} &= \frac{V_{\text{tot}}}{52} \times \frac{\text{pop}_p}{\sum_{p'} \text{pop}_{p'}} \times \frac{10}{18} \frac{\text{pop}_{<18}}{\sum_{p'} \text{pop}_{p'}}, \\
v^*_{2,p} &= \frac{V_{\text{tot}}}{52} \times \frac{\text{pop}_p}{\sum_{p'} \text{pop}_{p'}} \times \frac{\left(\sum_{p'} \text{pop}_{p'} - \text{pop}_{<11}\right)}{\sum_{p'} \text{pop}_{p'}},
\end{aligned}$$

for $p = 1, \ldots, P$. We obtain the weekly per-capita vaccination rate as such: $v_{a,p} = \frac{v^*_{a,p}}{\text{pop}_{a,p}}$ for $p = 1, \ldots, P$ and $a = 0, 1, 2$.

B Model Fitting: Estimates

Estimator	$\hat{\beta}_1^0$	$\hat{\beta}_2^0$	$\hat{\beta}_3^0$	$\hat{\beta}_4^0$	$\hat{\beta}_1^1$	$\hat{\beta}_2^1$	$\hat{\beta}_3^1$	$\hat{\beta}_4^1$
$\hat{\Theta}^{\text{SSE}}/\hat{\Theta}^{\text{MLE}_{\text{Poi}}}$	0.34	0.22	0.35	0.38	5.52	6.56	3.76	2.59
$\hat{\Theta}^{\text{MLE}_{\text{NB}}}$	0.40	0.40	0.41	0.43	0.93	0.47	1.31	0.95

Table 2: Baseline transmission and Gaussian amplitude parameters $\hat{\beta}_{1:P}^0$ and $\hat{\beta}_{1:P}^1$ for $p = 1, \ldots, 4$ under different estimation approaches.

Estimator	$\hat{\sigma}_1^G$	$\hat{\sigma}_2^G$	$\hat{\sigma}_3^G$	$\hat{\sigma}_4^G$	$\hat{\phi}_1$	$\hat{\phi}_2$	$\hat{\phi}_3$	$\hat{\phi}_4$	$\hat{\kappa}_1$	$\hat{\kappa}_2$	$\hat{\kappa}_3$	$\hat{\kappa}_4$
$\hat{\Theta}^{\text{SSE}}/\hat{\Theta}^{\text{MLE}_{\text{Poi}}}$	5.29	10.01	6.68	6.25	113.24	129.30	129.81	123.25	–	–	–	–
$\hat{\Theta}^{\text{MLE}_{\text{NB}}}$	16.54	26.31	11.56	14.22	14.47	31.45	8.75	1.03	1.88	1.96	4.24	3.96

Table 3: Gaussian width $\hat{\sigma}_{1:P}^G$, Gaussian centre $\hat{\phi}_{1:P}$, and dispersion $\hat{\kappa}_{1:P}$ (only for negative-binomial) for $p = 1, \ldots, 4$ under different estimation approaches.

C Sensitivity Analysis: Additional

C.1 Gaussian centres ϕ_p

We examine how changes to the Gaussian centre parameters $\hat{\phi}_p$ affect the peaks of the predicted mean number of reported weekly infections across the $p = 1, \ldots, 4$ regions. Specifically, we scale each centre multiplicatively by $\rho^{\hat{\phi}_p} \in [0.5, 1.3]$ - that is, we vary $\hat{\phi}_p$ by taking fractions of what it was estimated to be in Section 6.2. Figure 8 illustrates how changes in $\hat{\phi}_p$ influence $\max\{\hat{\mu}_1\}, \max\{\hat{\mu}_2\}, \max\{\hat{\mu}_3\}$ and $\max\{\hat{\mu}_4\}$.

Panel (a) (Northeast, $p = 1$): Increasing $\hat{\phi}_1$ monotonically reduces the peaks in all regions. *Panel (b) (Midwest, $p = 2$):* As $\hat{\phi}_2$ increases, the Midwest peak decreases up to approximately $0.95\,\hat{\phi}_2$ and then rises thereafter. Because the Midwest exhibits near-negligible outflow in the migration matrix $\boldsymbol{Mi}(a)$, the induced changes in the other regions' peaks are small and visible mainly over $\rho^{\hat{\phi}_p} \in [0.5, 0.7]$. *Panel (c) (West, $p = 3$):* Increasing $\hat{\phi}_3$ reduces all regions' peaks up to about $0.95\,\hat{\phi}_3$; beyond this point, further increases primarily elevate the West peak, with limited impact elsewhere. *Panel (d) (South, $p = 4$):* Varying $\hat{\phi}_4$ affects only the South's peak, consistent with the zero-outflow migration of the South; peaks in the Northeast, Midwest, and West remain unchanged.

Finally, peak timing behaves as expected: the peak times only change for region p if $\hat{\phi}_p$ changes - as it should, seeing as $\hat{\phi}_p$ directly controls when the peak should occur. Changes in $\hat{\phi}_p$ have no effect on the peak times for other regions $p' = 1, \ldots, P$ for $p' \neq p$ however.

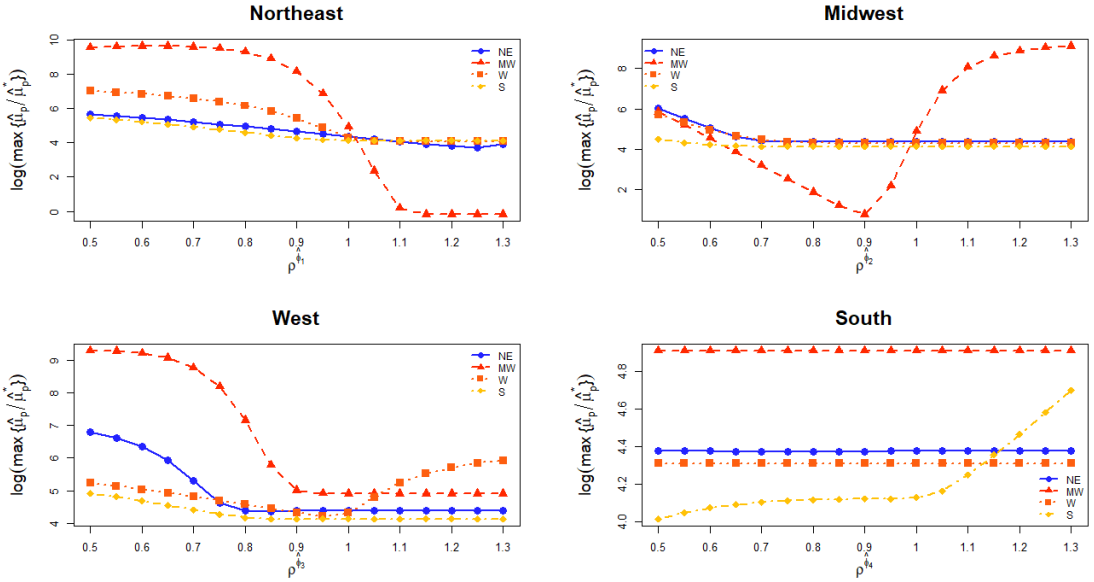

Figure 8: $\log\left(\max\left\{\frac{\hat{\mu}_p}{\hat{\mu}_p^*}\right\}\right)$ vs $\rho^{\hat{\phi}_p}$ for $p = 1, \ldots, P$ regions.

D Pertussis Model Assumptions

D.1 States and clinical course

- Symptomatic, untreated individuals $C^{\bar{T}}$ may only recover after first losing symptoms (they transition to As before R).

- Treated individuals T are assumed noninfectious immediately upon entering T.
- Asymptomatic infections As are infectious but with reduced infectiousness relative to symptomatic cases (fixed weight $\zeta^A_{a,p} \in (0, 1]$).
- Only As, $C^{\bar{T}}$, and C^T contribute to transmission; E, T, R, M, V, S do not.
- No co-infection or super-infection; one infection at a time.

D.2 Births and maternal immunity

- A constant fraction $\pi_{0,p}$ of newborns enter M (maternal immunity); the remainder enter S (if $\pi_{0,p} = 0$, this collapses to: all born are susceptible).
- Protection from maternal immunity is complete and homogeneous within M (no partial protection while in M).
- M exists only for the infant band ($a = 0$).
- Maternal immunity wanes deterministically at rate $\omega^M_{0,p}$; and any infant remaining in M upon aging out of $a = 0$ moves directly to S (no M beyond age < 1 years).
- No vertical transmission of infection; all births are uninfected.

D.3 Vaccination

- Vaccination moves $S \to V$ at rate $v_{a,p}$; no serologic testing is performed prior to vaccination (prior infection status is not checked).
- Vaccine action is modeled as 'leaky': susceptibility is reduced by efficacy $\epsilon_{a,p}$; once infected, vaccines do not alter duration or infectiousness unless stated.
- Loss of vaccine protection is complete: $V \to S$ at rate $\omega^V_{a,p}$ (no residual partial immunity).

D.4 Natural immunity

- Recovery confers complete, temporary immunity: $As \to R$ or $C^{\bar{T}} \to R$ then $R \to S$ at rate $\omega^R_{a,p}$ (all loss of immunity is complete).
- Waning rates $\omega^M_{0,p}$, $\omega^V_{a,p}$, $\omega^R_{a,p}$ are homogeneous within each (a, p) population.

D.5 Treatment-seeking

- Asymptomatic infectious $C^{\bar{T}}$ may only recover if they become asymptomatic first.

D.6 Transmission and mixing

- Individuals in age band a and patch p mix only within their own group; in other words, cross-age and cross-regional interactions - (a, p) with (a', p') for $a \neq a'$ or $p \neq p'$ - are assumed negligible.

D.7 Demography

- Aging, births, and deaths act on all compartments unless excluded; rates apply equally to any individual in age band a and patch p.
- M is removed at aging from $a = 0$; other compartments age forward without changing state.

D.8 Process

- Total population is conserved (apart from births/deaths/migration); all compartment sizes remain non-negative.
- Parameters are constant within (a, p) over $t \in [0, 187]$ unless explicitly time-varying (like $\lambda_{a,p}(t)$).

D.9 Drug-Resistance

- Resistant infections remain infectious under macrolide therapy - $C^{T,\text{Res}}$ does not enter the noninfectious treated population T.
- $C^{T,\text{Res}}$ may not switch to an effective alternative treatment (TMP-SMX for example) and move back to $T_{a,p}$.

References

Acosta, A. M., DeBolt, C., Tasslimi, A., Lewis, M., Stewart, L. K., and et al. (2015). Tdap vaccine effectiveness in adolescents during the 2012 washington state pertussis epidemic. *Pediatrics*, 135(6):981–989.

Bisgard, K. M., Pascual, F. B., Ehresmann, K. R., Miller, C. A., Cianfrini, C., Jennings, C. E., Rebmann, C. A., Gabel, J., Schauer, S. L., and Lett, S. M. (2004). Infant pertussis: who was the source? *Pediatrics*, 112(5):1069–1077.

Carbonetti, N. H. (2010). Pertussis toxin and adenylate cyclase toxin: key virulence factors of *Bordetella pertussis* and cell biology tools. *Future Microbiology*, 5(3):455–469.

Centers for Disease Control and Prevention (2005). Recommended antimicrobial agents for the treatment and postexposure prophylaxis of pertussis. https://www.cdc.gov/mmwr/preview/mmwrhtml/rr5414a1.htm. MMWR Recommendations and Reports; Accessed 2025-09-09.

Centers for Disease Control and Prevention (2024a). Infection control: *Bordetella pertussis*. https://www.cdc.gov/infection-control/hcp/healthcare-personnel-epidemiology-control/pertussis.html. Accessed 2025-09-09.

Centers for Disease Control and Prevention (2024b). National notifiable diseases surveillance system (nndss) weekly data. https://data.cdc.gov/NNDSS/NNDSS-Weekly-Data/x9gk-5huc. Accessed: September 10, 2025.

Centers for Disease Control and Prevention (2024c). Pertussis vaccination recommendations. https://www.cdc.gov/pertussis/hcp/vaccine-recommendations/index.html. Accessed 2025-09-09.

Centers for Disease Control and Prevention (2024d). Treatment of pertussis (whooping cough). https://www.cdc.gov/pertussis/hcp/clinical-care/index.html. Accessed 2025-09-09.

Centers for Disease Control and Prevention (2024e). Vaccinating pregnant patients: Tdap vaccine recommendations. Accessed: 2025-08-30.

Centers for Disease Control and Prevention (2025). Pertussis surveillance and trends. https://www.cdc.gov/pertussis/php/surveillance/index.html. Accessed 2025-09-09.

Centers for Disease Control and Prevention (CDC) (2025a). Provisional number of births, united states, 2024. Technical report, National Vital Statistics System, National Center for Health Statistics. Available at: https://www.cdc.gov/nchs/nvss/vsrr/provisional-tables.htm.

Centers for Disease Control and Prevention (CDC) (2025b). Provisional number of deaths, united states, 2024. Technical report, National Vital Statistics System, National Center for Health Statistics. Available at: https://www.cdc.gov/nchs/nvss/vsrr/provisional-tables.htm.

Chit, A., Zivaripiran, H., Shin, T., Mould-Quevedo, J., Kraicer-Melamed, H., and Jacobsen, M. (2018). Acellular pertussis vaccine effectiveness over time: A systematic review, meta-analysis, and modeling study. *PLoS ONE*, 13(6):e0197970.

Diavatopoulos, D. A., Cummings, C. A., Schouls, L. M., and et al. (2005). Characterization of a highly conserved island in the genome of *Bordetella pertussis* that is absent from *Bordetella bronchiseptica*. *PLoS Pathogens*, 1(3):e45.

European Centre for Disease Prevention and Control (2024). Increase of pertussis cases in the eu/eea. https://www.ecdc.europa.eu/en/publications-data/increase-pertussis-cases-eueea. Published 2024-05-08; Accessed 2025-09-09.

Evans, C. M., Linley, L., Vickers, M., Clark, T. A., and Skoff, T. H. (2023). Diagnostic delay and age in pertussis patients: implications for timely treatment. *Clinical Infectious Diseases*, 76(5):e1142–e1150.

Feng, Y., Zou, M., Chen, H., Yang, W., and Liu, Y. (2021). Emerging macrolide resistance in Bordetella pertussis. *The Lancet Microbe*, 2(9):e489–e490.

Guris, D., Strebel, P. M., Bardenheier, B., Brennan, M., Tachdjian, R., Finch, E., and Wharton, M. (1999). Changing epidemiology of pertussis in the united states: increasing reported incidence among adolescents and adults, 1990–1996. *Clinical infectious diseases*, 28(6):1230–1237.

Klein, N. P., Bartlett, J., and et al. (2012). Waning protection after fifth dose of acellular pertussis vaccine in children. *New England Journal of Medicine*, 367(11):1012–1019.

Klein, N. P., Bartlett, J., Fireman, B., and Baxter, R. (2016). Comparative effectiveness of acellular versus whole-cell pertussis vaccines in teenagers. *Pediatrics*, 137(5):e20152970.

Lavine, J. S., King, A. A., and Bjornstad, O. N. (2011). Short-lived immunity against pertussis, age-specific routes of transmission, and the utility of a teenage booster vaccine. *Vaccine*, 29(1):108–114.

Miller, E., Greenberg, D. P., Mothner, B., and Yurdakök, K. (2014). Waning immunity and its influence on pertussis control. *Journal of Infectious Diseases*, 209(Suppl_1):S20–S26.

Regan, A. K., Wood, N., Macartney, K., McIntyre, P., Moher, D., and et al. (2018). Effectiveness of maternal vaccination with tdap in preventing pertussis infection in young infants: A case–control study. *Clinical Infectious Diseases*, 66(8):1216–1221.

Skoff, T. H., Blain, A., Watt, J., and et al. (2017). Effectiveness of vaccination during pregnancy to prevent infant pertussis. *Pediatrics*, 139(5):e20164091.

U.S. Census Bureau (2024a). Vintage 2024 population estimates by u.s. census region. Available at: https://www.census.gov/popclock/data$_t$*ables.php?component* = *growth*.

U.S. Census Bureau (2024b). Vintage 2024 population estimates: National, state, and regional components of change. Includes births, deaths, and net domestic migration by region for July 2023–June 2024. Available at: https://www.census.gov/programs-surveys/popest.html.

U.S. Health Resources and Services Administration (2018). National vaccine injury compensation program data reports. Reported 503,068,145 pertussis-containing vaccine doses administered, 2006–2017.

Wang, Z., Li, X., and Hu, Y. (2021). Macrolide resistance in *bordetella pertussis*: Current status and future concerns. *Frontiers in Microbiology*, 12:653.

Warfel, J. M., Zimmerman, L. I., and Merkel, T. J. (2014). Acellular pertussis vaccines protect against disease but fail to prevent infection and transmission in a nonhuman primate model. *Proceedings of the National Academy of Sciences of the United States of America*, 111(2):787–792.

Wendelboe, A. M., Van Rie, A., Salmaso, S., and Englund, J. A. (2005). Duration of immunity against pertussis after natural infection or vaccination. *Pediatric Infectious Disease Journal*, 24(5 Suppl):S58–S61.

Wirsing von Konig, C. H. (2005). Epidemiology of pertussis: a comparison across age groups. *Pediatric Infectious Disease Journal*, 24(5):S19–S24.

Wiuff, A., Brown, D., Lamagni, T., and Crowcroft, N. (2005). Effectiveness of macrolide treatment in pertussis: a systematic review. *The Journal of Antimicrobial Chemotherapy*, 56(3):357–363.

Wright, S. W. (1995). Pertussis: epidemiology and control. *The Pediatric infectious disease journal*, 14(5):446–457.

Yeung, K. H. T., Duclos, P., Nelson, E. A. S., and Hutubessy, R. C. W. (2017). An update of the global burden of pertussis in children younger than 5 years: a modelling study. *The Lancet Infectious Diseases*, 17(9):974–980.